Monte Carlo simulation of a compact microbeam radiotherapy system based on carbon nanotube field emission technology

Eric C. Schreiber[a] and Sha X. Chang
Department of Radiation Oncology, University of North Carolina, Chapel Hill, North Carolina 27599

(Received 22 December 2011; revised 17 May 2012; accepted for publication 24 May 2012; published 16 July 2012)

Purpose: Microbeam radiation therapy (MRT) is an experimental radiotherapy technique that has shown potent antitumor effects with minimal damage to normal tissue in animal studies. This unique form of radiation is currently only produced in a few large synchrotron accelerator research facilities in the world. To promote widespread translational research on this promising treatment technology we have proposed and are in the initial development stages of a compact MRT system that is based on carbon nanotube field emission x-ray technology. We report on a Monte Carlo based feasibility study of the compact MRT system design.
Methods: Monte Carlo calculations were performed using EGSnrc-based codes. The proposed small animal research MRT device design includes carbon nanotube cathodes shaped to match the corresponding MRT collimator apertures, a common reflection anode with filter, and a MRT collimator. Each collimator aperture is sized to deliver a beam width ranging from 30 to 200 μm at 18.6 cm source-to-axis distance. Design parameters studied with Monte Carlo include electron energy, cathode design, anode angle, filtration, and collimator design. Calculations were performed for single and multibeam configurations.
Results: Increasing the energy from 100 kVp to 160 kVp increased the photon fluence through the collimator by a factor of 1.7. Both energies produced a largely uniform fluence along the long dimension of the microbeam, with 5% decreases in intensity near the edges. The isocentric dose rate for 160 kVp was calculated to be 700 Gy/min/A in the center of a 3 cm diameter target. Scatter contributions resulting from collimator size were found to produce only small (<7%) changes in the dose rate for field widths greater than 50 μm. Dose vs depth was weakly dependent on filtration material. The peak-to-valley ratio varied from 10 to 100 as the separation between adjacent microbeams varies from 150 to 1000 μm.
Conclusions: Monte Carlo simulations demonstrate that the proposed compact MRT system design is capable of delivering a sufficient dose rate and peak-to-valley ratio for small animal MRT studies.
 [http://dx.doi.org/10.1118/1.4728220]

Key words: microbeam, small animal irradiator, Monte Carlo

I. INTRODUCTION

In recent decades, a revolution in radiotherapy technology has significantly improved anatomical radiation targeting accuracy and radiation dose distribution optimization.[1–4] Intensity-modulated radiotherapy and image-guided radiotherapy are widely used and have been shown to produce equal/better local tumor control with fewer treatment side effects.[5–7] However, the Holy Grail of eradicating tumor without harming surrounding normal tissue still seems unapproachable for many types of cancer patients, especially those with large tumors, ill-defined tumor volumes, and/or nearby radiosensitive normal tissues, including many pediatric cancer patients.[8] An ideal radiotherapy approach would need to have intrinsic selectivity to tissue type—eradicating tumor cells while leaving normal tissue function undamaged under the same radiation. Microbeam radiation therapy (MRT) is an experimental radiotherapy that has shown such tissue type selectivity in animal studies.[9–12] So far only a few synchrotron facilities in the world are capable of generating the unique spatial and temporal patterns of MRT radiation.[13] Further, the radiobiological mechanisms involved are still not well understood.[13] The lack of widely available MRT delivery systems hinders the progress of studies of the MRT mechanism now and of clinical application in the future. Our multidisciplinary research group has pioneered a compact MRT device using a nanotechnology-enabled x-ray tube technology.[14] This compact MRT technology is currently in the early phase of device development, testing, and feasibility demonstration. In this paper, we report the progress of one aspect of the technology development—Monte Carlo study of the proposed compact MRT irradiation system.

I.A. Microbeam radiotherapy

MRT is distinctly different from all conventional forms of radiotherapy in terms of its spatial dose distribution pattern, total dose, and dose rate. Typical MRT treatments deliver microscopically discrete spatial dose distributions: 10–100 μm wide parallel beams with a separation of several hundred microns between adjacent beams. MRT treatments generally consist of a single fraction, as opposed to the 5–30 fractions delivered in conventional radiotherapy and

radiosurgery treatments. The maximum entrance dose for a single fraction MRT treatment is in the range of 100–1000 Gy delivered at a dose rate of 100s Gy/s. Although not well known, MRT is not a new experimental radiotherapy technique.[15] A recent review paper by Brauer-Krisch *et al.*[13] has summarized the history of MRT technology development as well as developments in MRT radiobiology over the last two decades. Preclinical studies using different animal models have demonstrated that a single MRT treatment of hundreds of Gy peak dose can preserve normal tissue function, including that of the developing central nervous system.[10,13,16] Separate animal studies have shown that the same MRT radiation provided excellent tumor control.[9,10,12,17]

There are two major obstacles in translating MRT from research laboratories to clinical use: (1) the lack of comprehensive understanding of the underlying radiobiological mechanism and (2) the lack of widely available MRT irradiation systems. Currently, there are only a few MRT facilities in the world, such as the European Synchrotron Research Facility in France and the National Synchrotron Light Source, Brookhaven National Laboratory in the United States. No human MRT system exists today, although ESRF is in the process of developing such a system.[18] Because synchrotron-based MRT systems are massive in size and extremely costly, most cancer research groups are prevented from performing MRT research in their own laboratories, thus hindering the advancement of MRT mechanistic research and its potential clinical application.

I.B. Carbon nanotube field emission technology

Carbon nanotube (CNT) field emission is a new cathode approach to x-ray tube technology that has been pioneered by our nanomaterial research group.[19,20] Virtually all x ray or electron beam generating machines today, such as x-ray units, CT scanners, and medical linear accelerators rely on thermionic emission cathodes, where electrons are "boiled" off from a tungsten filament at very high temperatures. In field emission, cathode electrons are generated not by heat but by a quantum tunneling effect induced by the application of an external electric field.[19] The physics of field emission is summarized by the Fowler-Nordheim equation ($I = aV^2 \exp(-b\phi^{3/2}/\beta V)$), stating that emission current (I) increases exponentially with increasing field voltage (V) for a substance characterized by work function (ϕ), geometric enhancement factor (β) and constants (a and b).[19] Carbon nanotubes, due to their atomic-scale sharp tips and large aspect ratios, have a much larger field enhancement factor β and thus a much lower emission threshold field that is practical to achieve in compact devices ($\sim 10^2$ V/mm).

Compared to thermionic emission x-ray technology, field emission x-ray technology is capable of higher temporal resolution. CNT field emission technology makes the design of spatially distributed x-ray sources possible as CNT film cathodes can be in any form and shape, such as a segmented pixel cathode array. Each of the cathode segment/pixel can be individually programmable within the same x-ray tube.[21–24]

Our multidisciplinary research team has pioneered the development of a number of novel imaging and irradiation devices based on CNT field emission technology, including micro-CT,[25,26] multipixel stationary breast tomosynthesis,[27] multipixel stationary tomosynthesis for image-guided radiotherapy,[28] micro-CT-RT,[22] and image-guided single cell irradiation.[23,29] Based on the same nanotechnology, we propose a novel compact MRT irradiation system.[14]

I.C. CNT-technology enabled MRT system

We are in the process of developing a prototype compact MRT irradiation system and are conducting feasibility studies and technology exploration. There are significant technical differences between our proposed x-ray tube-based MRT radiation technology and that studied in existing synchrotron-based facilities. For instance, synchrotron MRT has practically no beam divergence and exhibits dose rates of 1000 Gy/s, which are unreachable by any x-ray tube technology. So far there is no evidence suggesting that such a high dose rate is biologically necessary for MRT. A theoretical study by Enzmann and Pelc indicated that dose rates below 1000 Gy/s could result in a blurred dose distribution in moving animal targets.[30] Although we have no knowledge on the degree of potential motion blur in future animal irradiation, we have shown that CNT-based x-ray systems are capable of at least 15 ms temporal-resolution gating that may significantly minimize any motion blur.[31–33] Additionally, CNT cathode technology is capable of much higher electron current densities compared to thermionic cathodes[34] and allows cathode shape to be customized according to need. For the reasons mentioned above, CNT-based x-ray technology is ideally suited for use in a compact MRT device. In the initial phase of our research, we are exploring the technical feasibility and constraints of this novel x-ray system. Monte Carlo simulation is a valuable tool to assist many aspects of the system design and, based on the radiation dosimetry it would produce, to predict system performance.

I.D. Monte Carlo simulation study

Monte Carlo techniques have been widely used for clinical and research radiation dosimetry studies including MRT dosimetry. Nettelbeck *et al.*[35] have studied the effect of synchrotron-based beam and collimator parameters on dose distribution and microbeam parameters using the Monte Carlo simulation code PENELOPE.[36] Prezado *et al.* have performed PENELOPE calculations to evaluate optimal beam energy[37] and collimator design[38] for the ESRF MRT facility. Polarization effects in synchrotron microbeams have been studied using GEANT (Refs. 39 and 40) and EGS-based simulation codes.[41,42] Siegbahn *et al.*[43] have found good agreement between PENELOPE microbeam calculations and Si-based strip detectors as well as with other Monte Carlo simulation codes. Monte Carlo simulation has also been successfully used to study electron microbeam dosimetry. Our group has successfully applied the Monte Carlo technique to assist in the design of an electron microbeam cellular irradiation device[23]

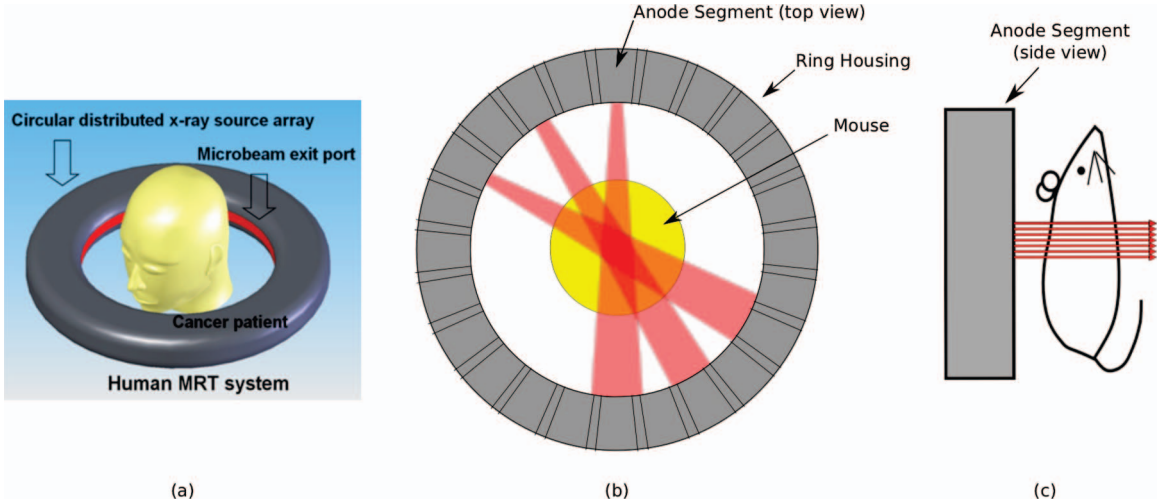

FIG. 1. Cartoon illustration of the proposed ring-design compact MRT system design. The design can scaled for small animal research and potential human therapy application. (a) Illustration of the basic concept of the compact MRT device in clinical use. The linear circular x-ray microbeam source is located within the circular x-ray tube housing. Power supplies, control electronics, and other supporting components of the MRT device are not shown. (b) A top view schematic of a segmented ring configuration consists of 24 linear segment sources equally spaced within the ring. For better clarity only beams from selected linear source segments are shown, emitting multiple planar microbeams as shown in (c). (c) A single linear segment anode, in which multiple parallel diverging microbeams are produced. The simulation reported in this article included up to 30 parallel planar microbeams.

and a small-animal IMRT delivery system[21] enabled by CNT technology.

In this paper, we report the results of a Monte Carlo simulation study evaluating the capabilities of the proposed compact MRT device. These results have been used to provide design guidance to the development of the prototype device.

II. METHODS AND MATERIALS

We have proposed a compact ring-shaped MRT system where each microbeam is generated from a segmented circular array of x-ray sources that surrounds the treatment object for small animal and potential human brain irradiation.[14] The basic design of a ring-shaped MRT system is illustrated in Fig. 1. Figure 1(a) shows a conceptual drawing of a distributed x-ray source in a ring configuration around a human patient's head. The circular x-ray source consists of a number of linear x-ray source segments, each of which generates microbeams irradiating the treatment object from a different direction. The carbon nanotube field emission x-ray source segments are individually addressable to differentially control the beam intensity if needed. Figure 1(b) shows a top view of multiple microbeams generated from selected linear source segments. The microbeams overlap at a lesion located at the center of the target. Each beam in Fig. 1(b) is a set of parallel planar microbeams emerging from a single anode segment as shown in Fig. 1(c). The MRT system relies on a circular linearly distributed x-ray source design to generate high photon fluence in the treatment target at the center of the MRT ring. Each of the microbeam planes is produced by generating electrons from a ring-shaped (or an array of linear segments) distributed CNT cathode, the electrons hitting a common reflection anode, and the resulting x-rays going through a MRT beam collimation system. Adjacent microbeam planes are generated the same way from additional arrays of linear CNT cathode segments on the ring system.

The proposed MRT system design can be reduced into many circular x-ray sources that each produces a single microbeam plane in the object at the center of the ring-shaped system. Each of the circular MRT x-ray sources can be divided further into many individual linear x-ray source segments arranged in a circle with the diameter of the MRT device. We start the simulation work with the basic unit of the MRT design, the linear CNT x-ray source, and finish it with the ring-shaped MRT system.

II.A. Basic CNT-MRT device design

The compact MRT device consists of parallel microbeam generating x-ray source segments. The schematic of the MRT segment used in this study is shown in Fig. 2. The segment consists of the following parts: a CNT-based cathode, focusing electrodes (in the microbeam width direction only), a tungsten anode, a vacuum chamber exit window, and an MRT collimator. In the prototype design studied in this project, the cathode, anode, and support devices are placed in a hexagonal vacuum chamber. The cathode is sized such that the projection of the electron beam on the anode matches the collimator size in both dimensions. The collimator opening is designed to produce a microbeam of 100 μm in width and 5–30 mm in length. A 200-μm thick steel exit window sits 4.5 cm from the center of the electron beam as it hits the anode. A 10 cm thick collimator is placed 5 mm outside of the vacuum chamber. While a much thinner collimator would be adequate for beam attenuation (a monoenergetic 160 keV beam has a TVL of 1.1 cm in copper), 10 cm thickness is necessary to prevent cross talk between adjacent microbeams.

The vacuum chamber and collimator thicknesses define a minimum source-to-surface distance (SSD) of 15 cm. The

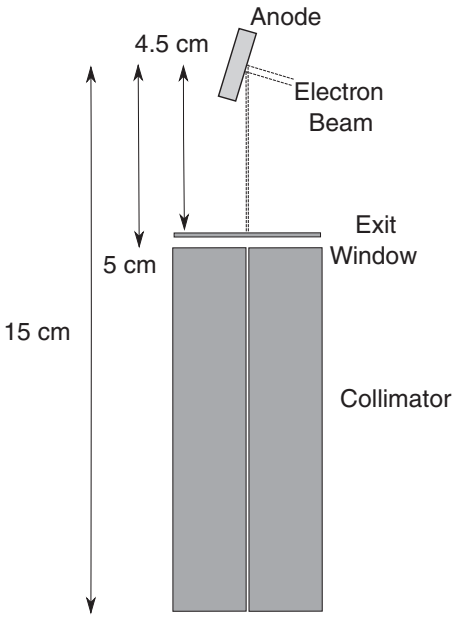

FIG. 2. Geometry of prototype single-direction microbeam MRT component used in Monte Carlo simulations. The 80-μm collimator aperture is not drawn to scale.

intention is to use this device for treatments at a constant source-to-axis distance (SAD). The minimum SAD for a 3 cm diameter mouse is therefore 16.5 cm. To allow some flexibility in the location of isocenter within the mouse model, the SAD was defined to be 18.5 cm.

The physical design of the prototype device requires a distance from the anode to the exit window no less than 4.5 cm, and a SSD to the target surface no less than 17.5 cm. The maximum anode voltage of the prototype device is 160 kVp.

II.B. Monte Carlo simulation

Radiation transport calculations in this work were carried out using EGSnrc-based Monte Carlo codes.[44] The EGSnrc code is the latest in a line of electromagnetic radiation transport simulations used in high-energy, nuclear, and medical physics, and contains many improvements over earlier versions (EGS4) that improve the accuracy of radiation transport down to 1 keV.[44] In particular, the 2009 release used in this project allowed some single-particle electron tracking, whereas previous versions of EGS used the continuous beam slowing model (CBSM), in which only aggregate effects of electron beams are used. This improves the accuracy of the dose calculations at the μm-level length scales necessary for studying microbeams. Calculations in the all portions of the x-ray device, including electron beam, anode, exit window, and collimator were performed using BEAMnrc, an EGSnrc-based radiotherapy simulation package. Dosimetry calculations were performed using the companion package DOSXYZnrc. Simulation parameters used for all calculations are shown in Table I.

The Monte Carlo simulations in this work are focused on direct calculation of a single plane microbeam and its dose deposition in the target. A superposition of multiple microbeam planes from different directions was used to study the dosimetric properties of the microbeam ring design. The simulation begins with a normal-incidence electron beam striking the tungsten anode as shown in Fig. 2. Two variance reduction techniques were used: directional bremsstrahlung splitting and selectively changing the electron cut-off energy. Directional bremsstrahlung splitting enhances the photon production calculation efficiency by repeating single bremsstrahlung events multiple times. The resulting photons are then weight adjusted and projected into a user-defined field.[45] The electron cut-off energy (ECUT) was set to 50 keV in the filter and collimator material to save calculation time by not tracking low-energy electrons outside the anode. The inclusion of the high-energy cutoff outside the anode produced no discernable difference in dose or fluence results.

Dose rate calculations were performed by simulating a cylindrical water phantom in DOSXYZnrc. The phantom was configured as a cylinder having a diameter and thickness of 3 cm (the diameter of an average mouse), with the calculated dose rate averaged over a voxel 1 mm $\times$ 1 mm $\times$ 10 μm in the central region of the microbeam. The particles produced by the BEAMnrc MRT device simulation were tallied as they exited the collimator and recorded in a phase space file containing each particle's type, energy, position, and direction. This phase space file was used to calculate 3D dose distributions in the water phantom and the mouse model. Phase space particles were recycled up to 20 times for each 3D dose calculation. These simulations were performed using DOSXYZnrc. Dose rate results were calculated in terms of cGy/incident electron and were renormalized to cGy/min/mA. All dose rate calculations assume dc emission current. Voxel dimensions varied depending on what property was being examined, but were typically 5 μm along the short dimension of the microbeam, 500 μm along the long dimension, and 1 mm in depth. All calculations were performed to a statistical uncertainty of 0.5% or better in the high-dose regions.

TABLE I. Summary of EGSnrc parameters used in the simulation of the compact microbeam radiotherapy device and phantom simulations.

Parameter	Value
Global ECUT	0.512
Global PCUT	0.001
Global SMAX	0.5
ESTEPE	0.25
XIMAX	0.5
Boundary crossing algorithm	PRESTA-I
Skin depth for BCA	0
Electron-step algorithm	PRESTA-II
Spin effects	On
Bremsstrahlung angular sampling	Koch and Motz
Bremsstrahlung cross sections	NIST
Bound Compton scattering	On
Pair angular sampling	Simple
Photoelectric angular sampling	On
Raleigh scattering	On
Atomic relaxations	On
Electron impact ionization	On

II.C. MRT system parameters studied

We performed MC simulation calculations for each of the major components of the compact MRT system including the cathode, anode, filter, collimator, and irradiation phantom in terms of material, geometry, x-ray beam energy, dose rate, and MRT-specific dose distribution.

II.C.1. Cathode

The cathode is modeled as a normal-incidence parallel rectangular beam impinging perpendicularly to the anode surface. Normal incidence is required for multiple beam operation. The electron beam size is selected to match the projection of the collimator on the anode surface. A larger cathode would produce photons unable to pass through the collimator opening. A smaller cathode would possibly produce a more uniform beam,[21] but would require an increased current density to achieve the same MRT photon fluence and would therefore require additional anode cooling for the same current. Electron focusing electrodes are used to focus the electron beam to a width of 1–2 mm before striking the anode. The effective microbeam source width after a 5°–20° anode angle is ∼100–200 μm. The electron beam energies studied were 100 kV and 160 kV. The Monte Carlo calculations in this study do not model the transport of the electron beam through the focusing electrodes, but begin with the electrons incident on the anode surface.

II.C.2. Anode

The anode angle was varied from 5° to 25° with respect to the central axis of the resulting x-ray beam. For a given photon beam size a smaller anode angle can increase the dose rate by using a larger electron spot size on the anode. But this can force photons to traverse a greater thickness of tungsten before leaving the anode, thus reducing the dose rate. The Monte Carlo results for angle selection were analyzed for their effect on beam symmetry and dose rate.

II.C.3. Exit window and collimator

X-ray sources typically use thin filters to remove low-energy x rays from the beam. The MRT x-ray tube vacuum chamber exit window also acts as a filter. The filter material and thickness options of 2 mm aluminum and 200- and 400-μm steel were studied.

The MRT collimator is designed to project a large ratio (small width and large length) microbeam at isocenter. Except where stated, simulations assumed a single-aperture collimator. Field size in the long dimension was defined to be 5–30 mm, with the narrow dimension varying from 50 to 200 μm at isocenter. Collimator openings are nondivergent. Multiple parallel microbeam configuration results are generated based on single microbeam simulation results.

There are two considerations in collimator thickness design: preventing cross talk between adjacent microbeams, and providing sufficient attenuation between adjacent beams. Cross talk can be minimized by having a large aspect ratio between collimator thickness and aperture width, and by placing the upstream edge of the collimator as close to the radiation source as possible. The physical design of the vacuum chamber in the prototype device requires the collimator be placed outside the chamber, at least 5 cm from the radiation source. Under these circumstances, the collimator thickness required to prevent cross talk is much thicker than necessary for attenuation purposes. The collimator material used in all calculations is copper.

II.C.4. Dose calculations in the phantom

All dose calculations were performed in a 3 cm diameter cylindrical water target centered 18.5 cm from the photon source. The variations in device components described above (including beam energy, anode angle, exit window material, and collimator geometry) were evaluated for their effect on dose rate, peak-to-valley ratio for adjacent beams, and beam divergence. Dose rate was evaluated at the phantom surface and at depth (isocenter).

III. RESULTS

III.A. Anode

Dose rate at the center of the microbeam vs anode angle is shown in Fig. 3. The dose rate is shown to be relatively constant between 10° and 25°. Below 10°, the dose rate begins dropping by more than 10%. Electron spot sizes on the anode are scaled such that the projection of the electron spot matches the collimator aperture. Current density on the anode surface, and hence the spontaneous anode heating, is therefore minimized for the smallest possible anode angle. Final dose calculations were performed assuming a 10° anode angle. No discernable heel effect through the collimator was observed for this anode angle as shown in Fig. 4(a). This is likely due to electron scatter blurring out any heel effect over the very narrow width of the collimator opening.

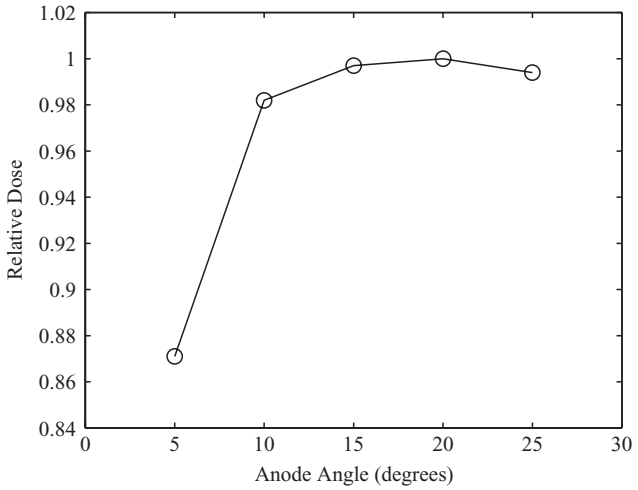

FIG. 3. Microbeam peak dose rate vs angle for 150-kVp configuration. The single direction microbeam width is 100 μm.

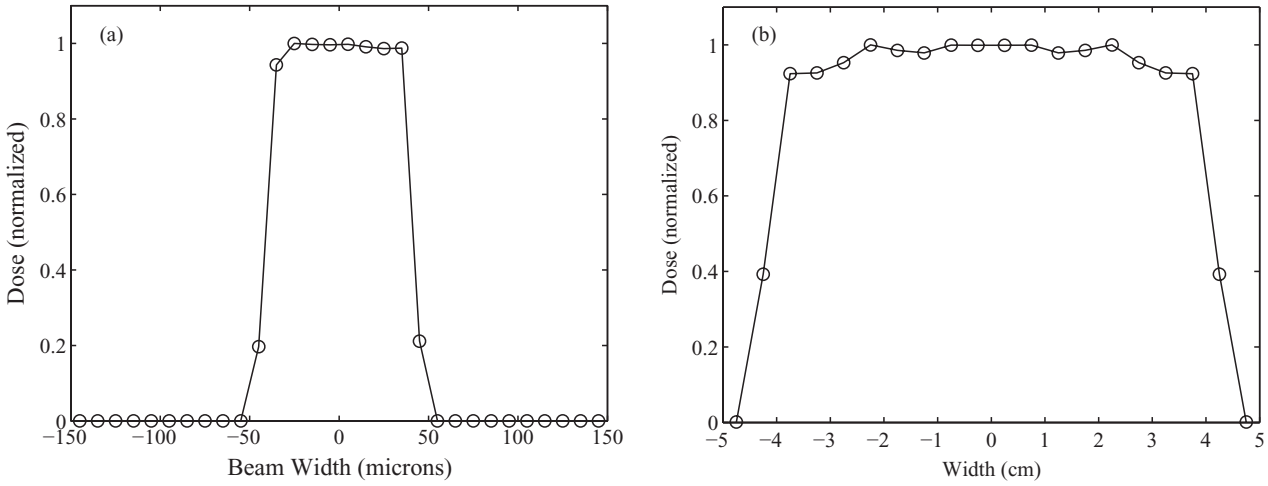

FIG. 4. Fluence distribution of photons emerging from MRT collimator for 10° anode angle. (a) The fluence distribution in the narrow dimension for an 80.6-μm wide collimator projecting to a 100-μm wide microbeam at isocenter. (b) The fluence in the long dimension for an 8.1 cm long extended collimator projecting to 10 cm at isocenter. The length of the microbeam can be defined by the length of the collimator aperture.

III.B. Exit window and collimator

Percentage depth dose (PDD) curves for the three different beam filtrations are shown in Fig. 5. The filter options were 2 mm Al, 200 μm Fe, and 400 μm Fe. Insufficient beam filtration would lead to excessive surface dose. The 200-μm steel exit window of the vacuum chamber produces similar beam hardness to the 2 mm aluminum filter at depth but has 10% less surface dose. Increasing the thickness of the steel exit window from 200 μm to 400 μm further reduces the surface dose.

Figure 4(a) shows negligible beam transmission through the copper collimator, indicating that the 10 cm thickness is sufficient to attenuate the x-ray beam. Small angle scattering near the edge of the collimator aperture may reduce the average beam energy, increasing surface dose and reducing the penetrating power of the beam. Figure 6 demonstrates that the energy spectrum of the x-rays do not substantially change as they pass through the microbeam collimator.

III.C. Dose distribution

For the 160-kVp configuration, the depth dose curve is shown in Fig. 5. Dose at isocenter can be estimated to be 60% of the dose at the surface. The lateral dose profile at 1.5 cm depth for a 100-μm wide microbeam is shown in Fig. 7. The dose profile is characterized by relatively sharp field edges and very low dose outside the field. When a multiple microbeam array is used for irradiation, the dose in the valley is the cumulative phantom scatter dose from each of the microbeams (Fig. 8). For a microbeam array that covers a 1 cm width perpendicular to the microbeams, the peak-to-valley ratio ranges from 10 to 100 as beam spacing varies from 150 to 500 μm for a microbeam width of 100 μm FWHM (Fig. 9).

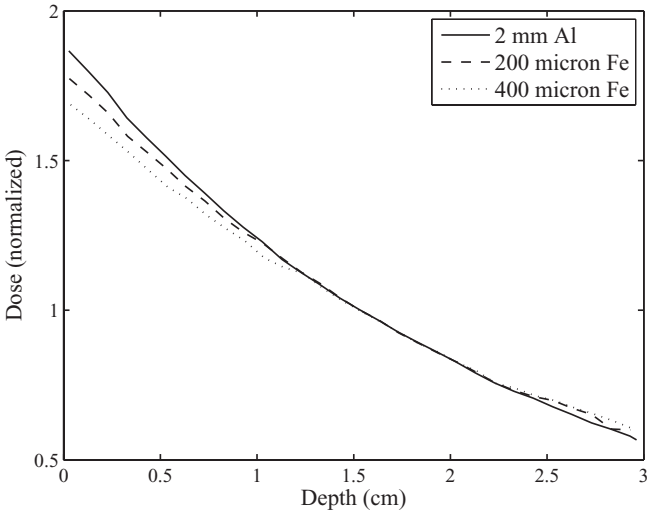

FIG. 5. Microbeam percentage depth dose of the MRT in the cylindrical water target for three different filtration thickness/materials.

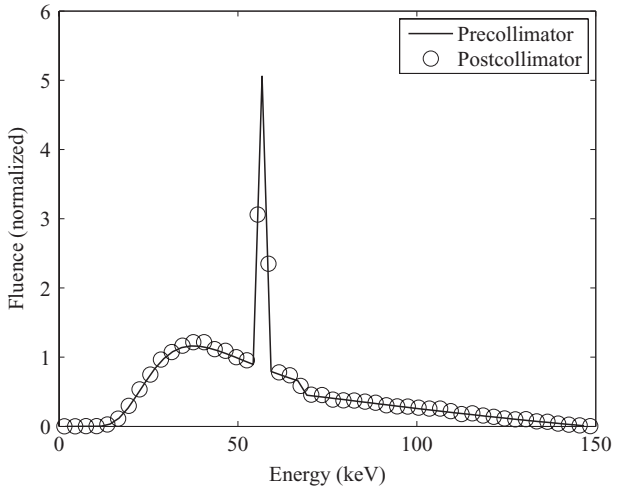

FIG. 6. Energy spectrum of a 150 kV beam before and after passing through the copper collimator. The narrow peak is a characteristic x-ray peak from the tungsten anode.

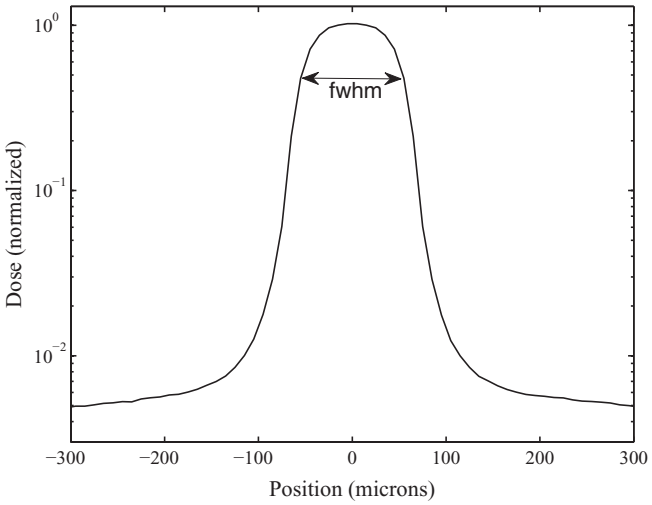

FIG. 7. Log-linear plot of the dose profile of a 160-kVp microbeam at 1.5 cm depth in a water target. The beam is collimated to form a 100-μm wide beam (FWHM) at 1.5 cm depth.

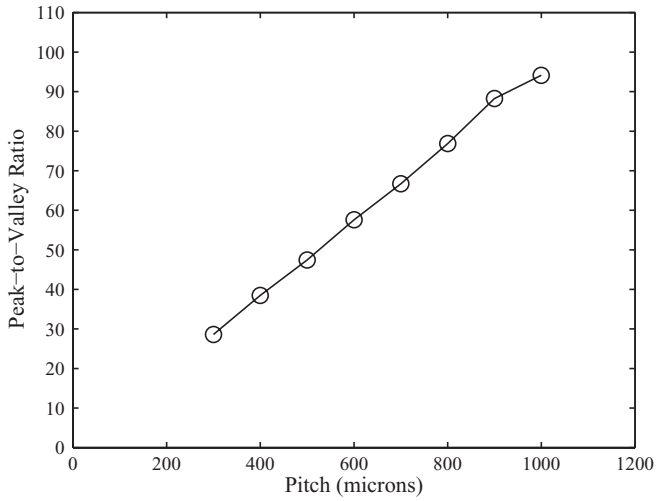

FIG. 9. Peak-to-valley ratio for a single direction microbeam array irradiating a 1 cm tumor at different separation distances between adjacent beams (pitch) as shown in Fig. 8.

Figure 10 shows the microbeam dose profile variation at beam attenuating depths of 5 mm, 15 mm, and 25 mm in a 30 mm diameter phantom. The corresponding microbeam width varied from 100 μm at depth of 5 mm to 120 μm at the depth 25 mm.

III.D. Dose rate

The dose rate varies with electron beam energy (E) according to the standard E^2 dependence of the bremsstrahlung equation. The dose at the center of the 3 cm diameter phantom for the 160 kV beam was calculated to be 1.9e-18 Gy per incident electron for a 100-μm microbeam generated by a 0.464 $\times$ 4 mm cathode. This corresponds to a dose rate of 700 Gy/A/min. This dose rate varies very little with collimator width (Fig. 11), indicating that photon scatter contributes relatively little to dose.

III.E. Ring design

The simulation results reported above describe single or parallel planar microbeams emerging from the same anode segment and entering the target from the same angle. We have simulated the dosimetry of the ring-design MRT shown in Fig. 1 using multiple instances of the single-direction microbeam simulation results at regular angle spacing. This ring design substantially increases the dose rate in the tumor, and the total dose in the tumor region relative to adjacent areas. The dose distribution obtained using a MRT ring design varies with number of beams chosen. Figure 12 shows the dose

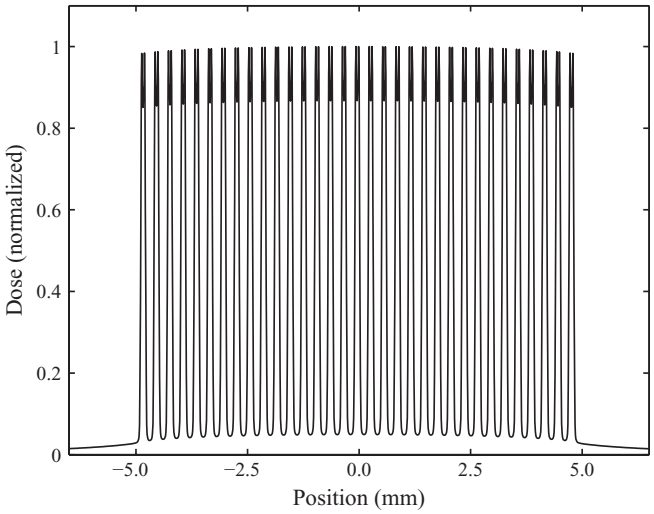

FIG. 8. Dose profile from multiple parallel 160 kV microbeams of 100-μm width at depth of 15 mm. The distribution covers 1 cm with 33 microbeams spaced 300 μm apart.

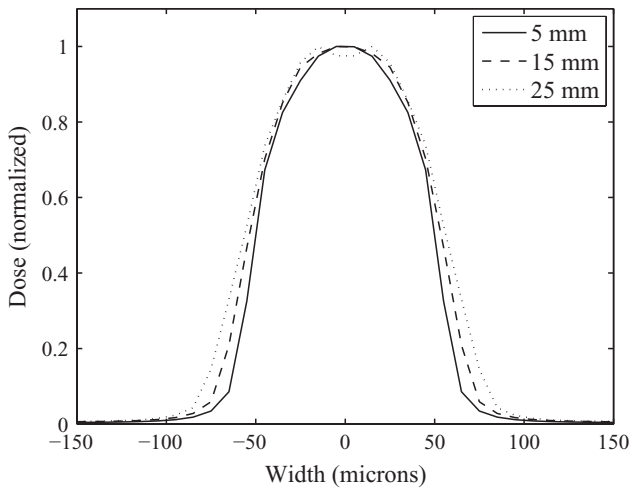

FIG. 10. Microbeam dose profiles at beam attenuating depths of 5 mm, 15 mm (phantom center), and 25 mm. The microbeam energy is 160 kV and the dose profile is simulated in a mouse phantom of 3 cm diameter.

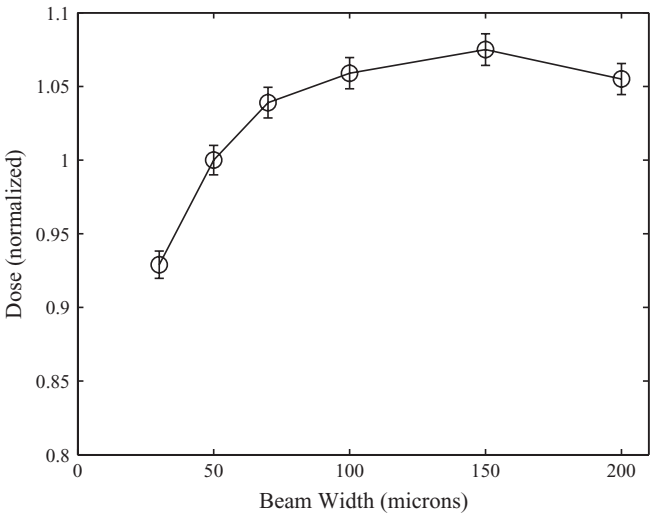

FIG. 11. Microbeam peak dose rate vs collimator (beam) width for the 160 kV single direction microbeam configuration. The dose rate for collimators 100 μm or larger is approximately constant within the statistical uncertainty.

distribution within the microbeam plane from the ring-design for 12 and 24 regularly spaced microbeam sources.

IV. DISCUSSION

We anticipate that future CNT MRT systems will be capable of energies higher than 160 kVp, but will likely still be lower energy that used at ESRF, which produces microbeam energies having mean and peak values of 100 and 500 keV, respectively.[37] One consequence of lower energy is a greater sensitivity to tissue inhomogeneities. For diagnostic-range photon energies, dose absorption in bone is enhanced relative to absorption in tissue due to increased photoelectric effect interactions, which is strongly dependent on the effective atomic number of the material. The degree of enhancement can be as high as a factor of four, as shown in our previous studies of similar devices.[21] This effect will be somewhat mitigated by the large number of beams from different entry directions utilized in the ring configuration. This is supported by recent work by Chow *et al.* which demonstrated that arc configurations for 100 kVp and 225 kVp beams lead to large dose differences in bone, but minimal differences at isocenter.[46]

A second consequence of lower average energy is a steeper depth dose curve. For a single beam, this can lead to a higher entrance dose relative to the dose received by a tumor located deep within the target. As shown in Fig. 5, the single direction microbeam entrance dose can be 80% higher than the prescribed tumor dose. While potentially problematic for single-beam configurations, this effect is strongly mitigated by the use of multiple beams surrounding the target in a ring configuration. As shown in Fig. 12(b), the entrance dose for a 24-beam configuration can be less than 10% of the dose received by the tumor.

The proximity of the radiation source (anode) to the treatment target implies that microbeam divergence could be significant across the depth of the target. Normalized dose profiles vs depth from a single direction microbeam are shown in Fig. 10. For the physical constraints of the prototype system (17 cm SSD, 3 cm diameter target), the maximum increase of beam size due to divergence is 20 μm for a 100-μm isocentric beam width. This value is much smaller than the proposed separation (300 μm) between adjacent microbeams. The divergence effect is further minimized in the proposed ring configuration, in which each of the microbeams overlaps with an opposing beam. The overlap of a microbeam with other microbeams that have widened due to the divergence effect could conceivably lead to the ring configuration exhibiting microbeam widths larger than would be found from a

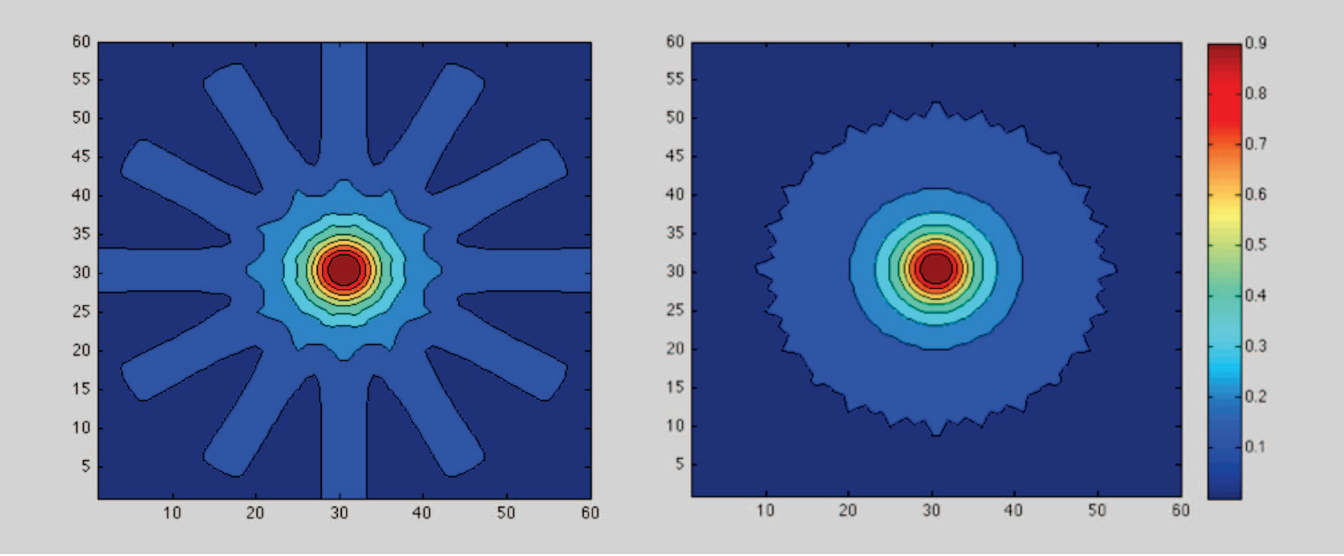

FIG. 12. Dose distributions within a microbeam plane for the ring-shaped source MRT design for 12 (left) and 24 (right) microbeam-direction configurations. Each microbeam is conformal in the long dimension of the beam to a 5 mm tumor at the center of a 30 mm diameter cylindrical target. The dose distributions displayed are within the plane of one of the microbeams. Dose profiles perpendicular to the microbeam plane are shown in Fig. 8.

single direction microbeam, as shown in Fig. 10. This effect is strongly mitigated, however, by the rapid dose falloff through the target of the opposing beam, leading to only a negligible increase in the cumulative microbeam width outside the center of the overlap region, where the intensities of opposing beams are comparable. The only observable impact of this effect is a small increase in the penumbra region in the center of the target, where all beams overlap. The small impact of this effect is included in the dose profiles and peak-to-valley ratios shown in Figs. 8 and 9. While the geometric effect of this divergence only weakly affects the peak-to-valley ratio, the biological effect of the beam widening is unclear. Previous studies[47] have suggested that the dose structure in the transition zone (on or near the penumbra of a single beam) may be important.

Finally, our study shows that the dose rate from a single 4 mm linear CNT cathode segment in the proposed compact MRT system is ~700 Gy/A/min. Target heating considerations are expected to limit the anode current to ~1 A per source segment for our prototype MRT tube design, leading to a theoretical dose rate limit of 700 Gy/min per segment source at isocenter. A 24-source ring configuration would therefore lead to an isocentric dose rate of 16 800 Gy/min or 280 Gy/s. For a typical MRT treatment dose of several hundreds Gy, the treatment delivery time would be a few seconds. This dose rate, while much higher than those used in conventional radiotherapy, is considerably below the 15 000 Gy/s reported at ESRF.[37] While the radiobiological impact of the MRT dose rate is still not well understood, the longer exposure times required by this device does raise the possibility of organ movement during beam delivery. If not managed, this effect could lead to an effective increase in beam width and valley dose and decrease in peak dose. Cao *et al.* have demonstrated that it is possible to eliminate the impact of cardiac motion in imaging the heart of a free breathing mouse during a 44 min session by respiratory and cardiac gating using a CNT field emission x-ray device.[31] We plan to use a similar gating technique for CNT-based MRT irradiation when organ motion is of concern.

V. CONCLUSIONS

The Monte Carlo study demonstrates that it is feasible for the compact carbon nanotube field emission-based MRT device to produce planar microbeams with some of the dosimetric features similar to those generated by synchrotron facilities. However, several differences between the proposed compact MRT device and the synchrotron-based MRT remain. These differences include energy spectrum, beam divergence, and dose rate. It remains to be investigated if these distinctions would lead to differences in any radiobiological endpoints. The estimated treatment delivery time of our compact MRT system design is several seconds for several hundred Gy of peak dose, compared to synchrotron-based MRT systems for which the delivery time can be a small fraction of a second. If necessary, we will rely on the demonstrated high temporal-resolution cardiac gating for MRT treatment delivery to minimize the potential motion-induced MRT dosimetry deterioration.

We have shown that the proposed compact MRT system design is capable of MRT dosimetry similar to that of the synchrotron based MRT for beam width of 100 μm in terms of dose distribution and peak-to-valley ratio. The proposed compact nanotechnology-enabled MRT system is not intended as a prototype for clinical use, but has the potential to greatly accelerate microbeam radiotherapy research by making the MRT treatment delivery technology for animal studies readily available to research laboratories outside the synchrotron facilities. MRT development for animal studies, if successful, may lead to the development of a system for clinical use.

ACKNOWLEDGMENTS

This work was supported by National Institutes of Health (NIH) Grant Nos. 1U54CA151652-01 and 5RC2CA148487-02. The authors want to thank Jian Zhang, Mike Hadsell, Jianping Lu, and Otto Zhou in the carbon nanotube field emission technology development team for their contributions to this project.

[a]Author to whom correspondence should be addressed. Electronic mail: erics@med.unc.edu

[1]T. Bortfeld, "IMRT: A review and preview," Phys. Med. Biol. **51**, R363–379 (2006).
[2]J. D. Fenwick, S. W. Riley, and A. J. Scott, "Advances in intensity-modulated radiotherapy delivery," Cancer Treat Res. **139**, 193–214 (2008).
[3]C. Yu, D. Shepard, M. Earl, D. Cao, S. Luan, C. Wang, and D. Z. Chen, "New developments in intensity modulated radiation therapy," Technol. Cancer Res. Treat. **5**, 451–464 (2006).
[4]K. K. Brock, "Image registration in intensity-modulated, image-guided and stereotactic body radiation therapy," Front Radiat. Ther. Oncol. **40**, 94–115 (2007).
[5]A. Pollack, A. Hanlon, E. M. Horwitz, S. Feinenberg, R. G. Uzzo, and R. A. Price, "Radiation therapy dose escalation for prostate cancer: A rationale for IMRT," World J. Urol. **21**, 200–208 (2003).
[6]M. J. Zelefsky, Z. Fuks, M. Hunt, Y. Yamada, C. Marion, C. C. Ling, H. Amols, E. S. Venkatraman, and S. A. Leibel, "High-dose intensity modulated radiation therapy for prostate cancer: Early toxicity and biochemical outcome in 772 patients," Int. J. Radiat. Oncol., Biol., Phys. **53**, 1111–1116 (2002).
[7]Q. Wu, M. Manning, R. Schmidt-Ullrich and R. Mohan, "The potential for sparing of parotids and escalation of biologically effective dose with intensity-modulated radiation treatments of head and neck cancers: A treatment design study," Int. J. Radiat. Oncol., Biol., Phys. **46**, 195–205 (2000).
[8]B. Knab and P. P. Connell, "Radiotherapy for pediatric brain tumors: When and how," Expert Rev. Anticancer Ther **7**, S69–77 (2007).
[9]P. Regnard, G. Le Duc, E. Brauer-Krisch, I. Tropres, E. A. Siegbahn, A. Kusak, C. Clair, H. Bernard, D. Dallery, J. A. Laissue, and A. Bravin, "Irradiation of intracerebral 9L gliosarcoma by a single array of microplanar x-ray beams from a synchrotron: Balance between curing and sparing," Phys. Med. Biol. **53**, 861–878 (2008).
[10]J. A. Laissue, G. Geiser, P. O. Spanne, F. A. Dilmanian, J. O. Gebbers, M. Geiser, X. Y. Wu, M. S. Makar, P. L. Micca, M. M. Nawrocky, D. D. Joel, and D. N. Slatkin, "Neuropathology of ablation of rat gliosarcomas and contiguous brain tissues using a microplanar beam of synchrotron-wiggler-generated x rays," Int. J. Cancer **78**, 654–660 (1998).
[11]F. A. Dilmanian, T. M. Button, G. Le Duc, N. Zhong, L. A. Pena, J. A. Smith, S. R. Martinez, T. Bacarian, J. Tammam, B. Ren, P. M. Farmer, J. Kalef-Ezra, P. L. Micca, M. M. Nawrocky, J. A. Niederer, F. P. Recksiek, A. Fuchs, and E. M. Rosen, "Response of rat intracranial 9L gliosarcoma to microbeam radiation therapy," J. Neuro-Oncol. **4**, 26–38 (2002).
[12]F. A. Dilmanian, G. M. Morris, N. Zhong, T. Bacarian, J. F. Hainfeld, J. Kalef-Ezra, L. J. Brewington, J. Tammam, and E. M. Rosen, "Murine EMT-6 carcinoma: High therapeutic efficacy of microbeam radiation therapy," Radiat. Res. **159**, 632–641 (2003).

[13]E. Brauer-Krisch, R. Serduc, E. A. Siegbahn, G. Le Duc, Y. Prezado, A. Bravin, H. Blattmann, and J. A. Laissue, "Effects of pulsed, spatially fractionated, microscopic synchrotron x-ray beams on normal and tumoral brain tissue," Mutat Res. **704**, 160–166 (2010).
[14]O. Zhou and S. Chang, U.S. patent #7220971 (2007).
[15]C. P. Baker, H. J. Curtis, W. Zeman, and R. G. Woodley, "The design and calibration of a deuteron microbeam for biological studies," Radiat. Res. **15**, 489–495 (1961).
[16]F. A. Dilmanian, G. M. Morris, G. Le Duc, X. Huang, B. Ren, T. Bacarian, J. C. Allen, J. Kalef-Ezra, I. Orion, E. M. Rosen, T. Sandhu, P. Sathe, X. Y. Wu, Z. Zhong, and H. L. Shivaprasad, "Response of avian embryonic brain to spatially segmented x-ray microbeams," Cell. Mol. Biol. (Noisy-le-grand) **47**, 485–493 (2001).
[17]A. Bouchet, B. Lemasson, G. Le Duc, C. Maisin, E. Brauer-Krisch, E. A. Siegbahn, L. Renaud, E. Khalil, C. Remy, C. Poillot, A. Bravin, J. A. Laissue, E. L. Barbier and R. Serduc, "Preferential effect of synchrotron microbeam radiation therapy on intracerebral 9L gliosarcoma vascular networks," Int. J. Radiat. Oncol. Biol. Phys. **78**, 1503–1512 (2010).
[18]H. Requardt, A. Bravin, Y. Prezado, E. Bräuer-Krisch, M. Renier, T. Brochard, P. Berkvens, F. Esteve, H. Elleaume, J. Adam, H. Blattmann, J. Laissue, B. Kaser-Hotz, C. Nemoz, and G. Berruyer, in *Proceedings of the 10th International Conference on Synchrotron Radiation Instrumentation 2009*, Melbourne, Australia, 2010 (unpublished).
[19]R. Gomer, *Field Emission and Field Ionization* (Harvard University Press, Cambridge, MA, 1961).
[20]Y. Cheng and O. Zhou, "Field emission from carbon nanotubes," C. R. Phys. **4**, 1021–1033 (2003).
[21]E. C. Schreiber and S. X. Chang, "Monte carlo simulation of an x-ray pixel beam microirradiation system," Radiat. Res. **171**, 332–341 (2009).
[22]S. Wang, S. Liu, L. An, O. Zhou, and S. Chang, "Fabrication and characterization of individually controlled multi-pixel carbon nanotube cathode array chip for micro-RT application for cancer research," Mater. Res. Soc. Symp. Proc. **1065**, QQ1004–1008 (2008).
[23]D. E. Bordelon, J. Zhang, S. Graboski, A. Cox, E. Schreiber, O. Z. Zhou, and S. Chang, "A nanotube based electron microbeam cellular irradiator for radiobiology research," Rev. Sci. Instrum. **79**, 125102 (2008).
[24]J. Zhang, G. Yang, Y. Z. Lee, Y. Cheng, B. Gao, Q. Qui, J. P. Lu, and O. Zhou, "A multi-beam x-ray imaging system based on carbon nanotube field emitters," Proc. SPIE **6142**, 614204 (2006).
[25]G. Z. Yue, Q. Qiu, B. Gao, Y. Cheng, J. Zhang, H. Shimoda, S. Chang, J. P. Lu, and O. Zhou, "Generation of continuous and pulsed diagnostic imaging x-ray radiation using a carbon-nanotube-based field-emission cathode," Appl. Phys. Lett. **81**, 355–357 (2002).
[26]J. Zhang, G. Yang, Y. Cheng, B. Gao, Q. Qiu, Y. Z. Lee, J. P. Lu, and O. Zhou, "A stationary scanning x-ray source based on carbon nanotube field emitters," Appl. Phys. Lett. **86**, 184104 (2005).
[27]D. Lalush, E. Quan, R. Rajaram, J. Zhang, J. P. Lu, and O. Zhou, "Tomosynthesis reconstruction from multi-beam x-ray sources," *Proceedings of the 3rd IEEE International Symposium on Biomedical Imaging: from Nano to Macro*, 1180–1183 (2006).
[28]J. S. Maltz, F. Sprenger, J. Fuerst, A. Paidi, F. Fadler, and A. R. Bani-Hashemi, "Fixed gantry tomosynthesis system for radiation therapy image guidance based on a multiple source x-ray tube with carbon nanotube cathodes," Med. Phys. **36**, 1624–1636 (2009).
[29]S. Chang, J. Zhang, D. Bordelon, E. Schreiber, A. Cox, and O. Zhou, "Development of a carbon nanotube based low-LET multi-pixel microbeam array single cell irradiation system," Radiat. Res. **166**, 658–659 (2006).
[30]D. R. Enzmann and N. J. Pelc, "Brain motion: Measurement with phase-contrast MR imaging," Radiology **185**, 653–660 (1992).
[31]G. Cao, Y. Z. Lee, R. Peng, Z. Liu, R. Rajaram, X. Calderon-Colon, L. An, P. Wang, T. Phan, S. Sultana, D. S. Lalush, J. P. Lu, and O. Zhou, "A dynamic micro-CT scanner based on a carbon nanotube field emission x-ray source," Phys. Med. Biol. **54**, 2323–2340 (2009).
[32]Y. Z. Lee, L. M. Burk, K. H. Wang, G. Cao, J. Volmer, J. Lu, and O. Zhou, "Prospective respiratory gated carbon nanotube micro computed tomography," Acad. Radiol. **18**, 588–593 (2011).
[33]L. M. Burk, Y. Z. Lee, S. Heathcote, K. Wang, W. Y. Kim, J. P. Lu, and O. Zhou, "carbon nanotube based respiratory gated micro-CT imaging of a murine model of lung tumors with optical imaging correlation," Proc. SPIE, **7965**, 79651L (2011).
[34]D. Shiffler, O. Zhou, C. Bower, M. LaCour, and K. Golby, "A high current, large area, carbon nanotube cathode," IEEE Trans. Plasma Sci. **32**, 2152–2154 (2004).
[35]H. Nettelbeck, G. J. Takacs, M. L. Lerch, and A. B. Rosenfeld, "Microbeam radiation therapy: A Monte Carlo study of the influence of the source, multislit collimator, and beam divergence on microbeams," Med. Phys. **36**, 447–456 (2009).
[36]J. Baro, J. Sempau, J. M. Fernandez-Varea, and F. Salvat, "PENELOPE: An algorithm for Monte Carlo simulation of the penetration and energy loss of electrons and positrons in matter," Nucl. Instrum. Methods B **100**, 31–46 (1995).
[37]Y. Prezado, S. Thengumpallil, M. Renier, and A. Bravin, "X-ray energy optimization in minibeam radiation therapy," Med. Phys. **36**, 4897–4902 (2009).
[38]E. Brauer-Krisch, H. Requardt, T. Brochard, G. Berruyer, M. Renier, J. A. Laissue, and A. Bravin, "New technology enables high precision multislit collimators for microbeam radiation therapy," Rev. Sci. Instrum. **80**, 074301 (2009).
[39]J. Stepanek, H. Blattmann, J. A. Laissue, N. Lyubimova, M. Di Michiel, and D. N. Slatkin, "Physics study of microbeam radiation therapy with PSI-version of Monte Carlo code GEANT as a new computational tool," Med. Phys. **27**, 1664–1675 (2000).
[40]J. Spiga, E. A. Siegbahn, E. Brauer-Krisch, P. Randaccio, and A. Bravin, "The GEANT4 toolkit for microdosimetry calculations: Application to microbeam radiation therapy (MRT)," Med. Phys. **34**, 4322–4330 (2007).
[41]M. De Felici, R. Felici, M. Sanchez del Rio, C. Ferrero, T. Bacarian, and F. A. Dilmanian, "Dose distribution from x-ray microbeam arrays applied to radiation therapy: An EGS4 Monte Carlo study," Med. Phys. **32**, 2455–2463 (2005).
[42]R. P. Hugtenburg, A. S. Adegunloye, and D. A. Bradley, "X-ray microbeam radiation therapy calculations, including polarisation effects, with the Monte Carlo code EGS5," Nucl. Instrum. Methods Phys. Res. A **619**, 221–224 (2010).
[43]E. A. Siegbahn, E. Brauer-Krisch, A. Bravin, H. Nettelbeck, M. L. Lerch, and A. B. Rosenfeld, "MOSFET dosimetry with high spatial resolution in intense synchrotron-generated x-ray microbeams," Med. Phys. **36**, 1128–1137 (2009).
[44]I. Kawrakow, "Accurate condensed history Monte Carlo simulation of electron transport. I. EGSnrc, the new EGS4 version," Med. Phys. **27**, 485–498 (2000).
[45]I. Kawrakow, D. W. Rogers, and B. R. Walters, "Large efficiency improvements in BEAMnrc using directional bremsstrahlung splitting," Med. Phys. **31**, 2883–2898 (2004).
[46]J. C. Chow, M. K. Leung, P. E. Lindsay, and D. A. Jaffray, "Dosimetric variation due to the photon beam energy in the small-animal irradiation: A Monte Carlo study," Med. Phys. **37**, 5322–5329 (2010).
[47]H. Blattmann, W. Burkard, V. Djonov, E. M. DiMichiel, E. Brauer, J. Stepanek, A. Bravin, J. O. Gebbers, and J. Laissue, "Microbeam irradiation in the chorio-allantoic membrane (CAM) of chicken embryo," Strahlenther. Onkol. **178**, 118 (2002).